Journal of Magnetism and Magnetic Materials 358-359 (2014) 16–22

Contents lists available at ScienceDirect

Journal of Magnetism and Magnetic Materials

journal homepage: www.elsevier.com/locate/jmmm

Density of states, optical and thermoelectric properties of perovskite vanadium fluorides Na_3VF_6

A.H. Reshak [a,b], Sikander Azam [a,*]

[a] New Technologies—Research Center, University of West Bohemia, Univerzitni 8, 30614 Pilsen, Czech Republic
[b] Center of Excellence Geopolymer and Green Technology, School of Material Engineering, University Malaysia Perlis, 01007 Kangar, Perlis, Malaysia

ARTICLE INFO

Article history:
Received 23 December 2013
Received in revised form
13 January 2014
Available online 25 January 2014

Keywords:
Electronic structure
Electronic charge density
Fermi surface
Optical properties
Thermal properties

ABSTRACT

The electronic structure, charge density and Fermi surface of Na_3VF_6 compound have been examined with the support of density functional theory (DFT). Using the full potential linear augmented plane wave method, we employed the local density approximation (LDA), generalized gradient approximation (GGA) and Engel–Vosko GGA (EVGGA) to treat the exchange correlation potential to solve Kohn–Sham equations. The calculation show that Na_3VF_6 compound has metallic nature and the Fermi energy (E_F) is assessed by overlapping of V-d state. The calculated density of states at the E_F are about 18.655, 51.932 and 13.235 states/eV, and the bare linear low-temperature electronic specific heat coefficient (γ) is found to be 3.236 mJ/mol-K^2, 9.008 mJ/mol-K^2 and 2.295 mJ/mol-K^2 for LDA, GGA and EVGGA, respectively. The Fermi surface is composed of two sheets. The chemical bonding of Na_3VF_6 compound is analyzed through the electronic charge density in the (1 1 0) crystallographic plane. The optical constants and thermal properties were also calculated and discussed.

1. Introduction

The $A_2BB'F_6$ and $A_3B'F_6$ types elpasolite and cryolite [$(A, B = Li, Na, K, Rb, Tl, NH_4)$ and $(B' = Al, Sc, V, Cr, Fe, Bi, Ga, Y, In, Ln)$] is broadly enquired owing to the intriguing functional phase transition at low temperature [1–4] and amazing characteristics for acting as host components for luminescent ions attributable to their wide range of wavelength transmission and low refractive index [5]. Alter et al. [6] utilized the conformist solid state technique to synthesize the Na_3VF6 (cryolite type) having the monoclinic symmetry with space group $P21/n$, which is isotypic with cryolite Na_3AlF_6. Massa et al. synthesized the $(NH_4)_2NaVF_6$ (elpasolite-type) compound in a platinum tube sealed under an inert atmosphere [7].

In addition to the functional investigations, numerous procedures were applied to the groundwork of the fluorides for instance solid-state reaction [8–10], sol–gel antecendent [11–14], flux growth [15,16], hydro- thermal process [17–21] and fused-salt electrolysis procedure [22]. Amidst them, the hydro thermal procedure presents an appealing choice for the synthesis of components that would generally be arranged with the customary high temperature solid-state procedures [23–24].

He et al. [25] studied the hydro thermal syntheses, structural characterization and magnetic studies of double perovskite vanadium fluorides $(NH_4)_2NaVF_6$ and Na_3VF_6.

In hydrothermal synthesis, the use of a solvent were carried out under somewhat gentle situation, would allow a fast blending of some chemical elements, premier to homogeneous goods with

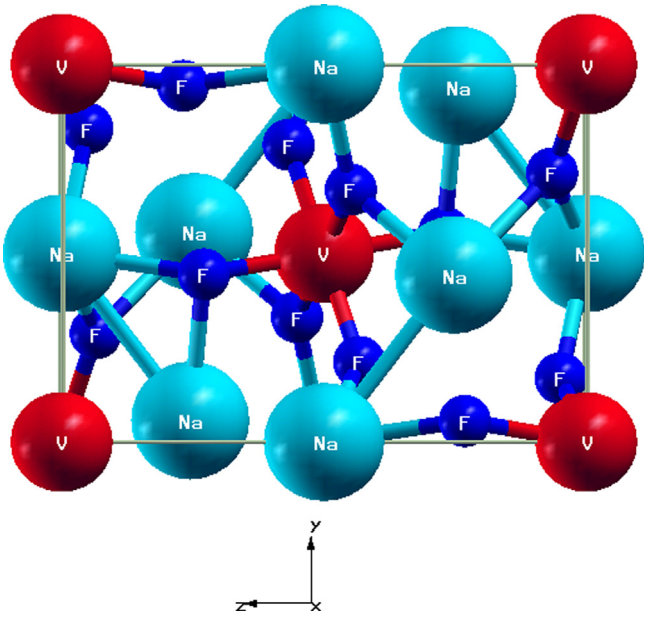

Fig. 1. Unit cell structure for Na_3VF_6 compound.

* Corresponding author. Tel.: +420775928620.
E-mail addresses: sikander.physicst@gmail.com, sikandar_hu@yahoo.com (S. Azam).

0304-8853/$ - see front matter © 2014 Elsevier B.V. All rights reserved.
http://dx.doi.org/10.1016/j.jmmm.2014.01.034

manageable particle dimensions, which is slightly tough to accomplish when using the high warmth solid-state technique.

The modest hydrothermal stipulations are also attractive in the formulation for crystals of rare earth and complex fluorides since they have the benefits such as reduced temperature obligation, one-step synthetic process, easy handling and controllable particle dimensions circulation. Under the modest hydrothermal status, complex fluorides, like perovskite-type fluorides $LiBaF_3$, $KMgF_3$ and the scheelite type fluorides $LiYF_4$, $NaYF_4$, KYF_4, and $BaBeF_4$, were also synthesized by the research group [26]. The researcher have also investigated the luminescence of lanthanide doping of these compounds [27,28]. As an elongation of our investigation, we also present the electronic structure, electronic charge density, optical and thermal properties of perovskite vanadium fluorides Na_3VF_6.

Table 1
Optimized atomic positions (Å) in comparison with the experimental data [25].

Atoms	*x* (Exp.)	*x* (Opt.)	*y* (Exp.)	*y* (Opt.)	*z* (Exp.)	*z* (Opt.)
V1	0	0.0000	0	0.0000	0	0.0000
Na1	0	0.0000	0	0.0000	0.5	0.5000
Na2	−0.006(8)	0.9902	0.4448(2)	0.4429	0.2586(9)	0.2548
F1	0.0826(6)	0.1604	0.2987(5)	0.2878	−0.0130(1)	0.9333
F2	0.0843(7)	0.1131	0.0913(8)	0.0554	0.2175(9)	0.2295
F3	0.8078(7)	0.7955	0.6298(4)	0.6689	0.4942(0)	0.4501

2. Methodology

The crystal structure of Na_3VF_6 compounds has shown in Fig. 1. The compound has the monoclinic structure with space group $P21/n$. The lattice constants for the Na_3VF_6 compound are $a=5.510(6)$ Å, $b=5.725(8)$ Å, $c=7.948(6)$ Å, $\beta=90.410(8)^\circ$ [25]. The optimized atomic positions in comparison with the experimental one [25] are shown in Table 1. Good agreement was found which confirms the precision of our calculation. The calculation for the self-consistent was conceded out by using Wien2k code [28] which is based on full-potential linear augmented plane wave method. LDA, GGA and EVGGA[29–31] approximations were depleted to treat the exchange correlation potential by solving Kohn–Sham equations. The sphere radii used were 1.68 au, 1.88 au and 1.49 au for V, Na and F, respectively. The well converged

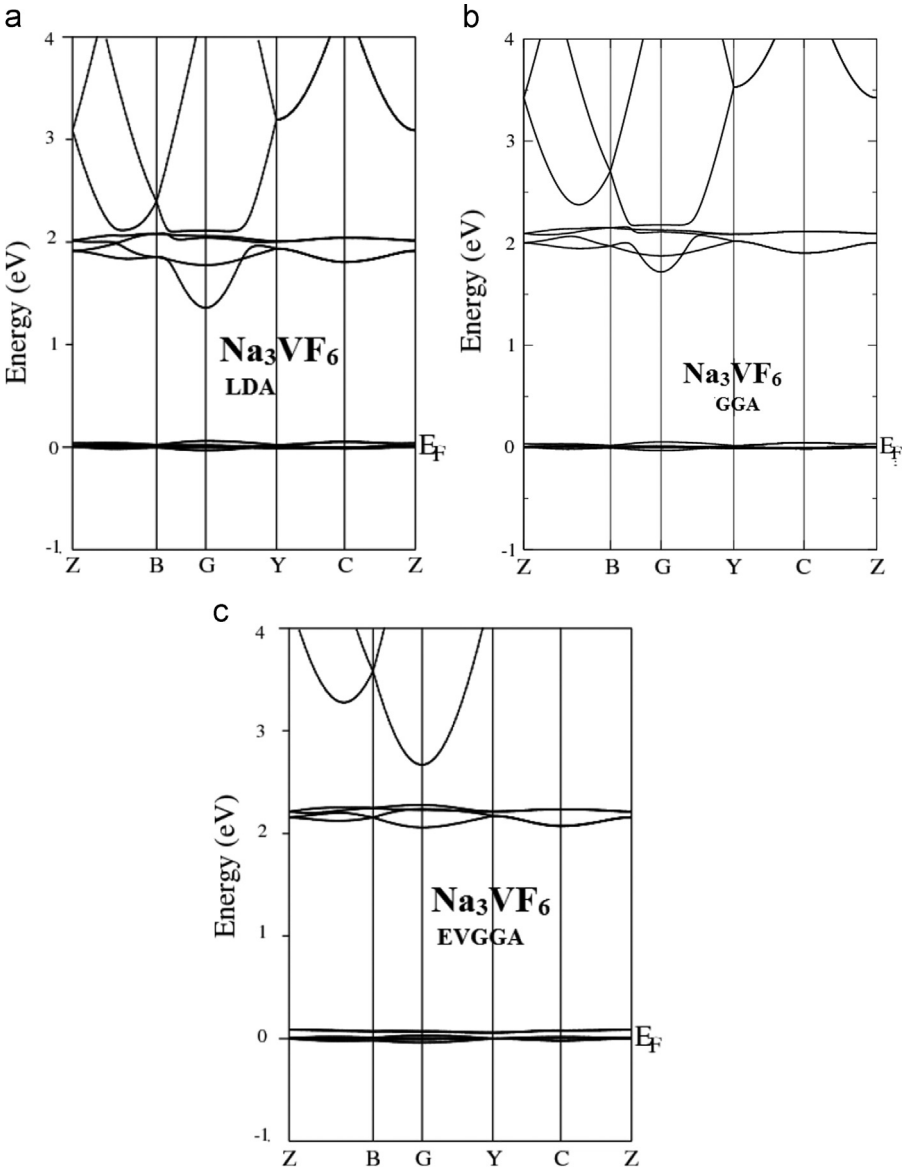

Fig. 2. Calculated band structures for LDA, GGA and EVGGA for Na_3VF_6 compound.

solutions obtained with $R_{MT}K_{max}=7.0$ (where R_{MT} is the smallest of the muffin-tin radii and K_{max} is the plane wave cut-off) and k-point sampling was checked.

For computing the optical properties, which frequently needs a dense mesh of consistently circulated k-points, the Brillouin zone integration was presented by means of the tetrahedron method with 1000k-points in the irreducible part of the Brillouin zone devoid of broadening. It is well known that the dielectric function $\varepsilon(\omega)$ is used to describe the optical response of the medium at all photon energies. In fact in metals, there exit two contributions to dielectric function occurring from the intraband and interband transitions. The interband transitions can be more cracked into direct and indirect transitions. Though, the intraband and indirect interband transitions involve phonon in sequence to account for the momentum transfer. The premeditated direct interband involvement to the imaginary part of the dielectric function, $\varepsilon(\omega)$, is computed by summing transitions from occupied to unoccupied states (with fixed k) over the Brillouin zone, weighted with the suitable matrix elements benevolent the chance for the transition. The imaginary part of the dielectric function $\varepsilon(\omega)$ is given as in Refs. [32–35]

$$\varepsilon_2^{ij}(\omega)=\frac{4\pi^2e^2}{Vm^2\omega^2}\times\sum_{knn'\sigma}\langle kn\sigma|p_i|kn'\sigma\rangle\langle kn'\sigma|p_j|kn\sigma\rangle \times f_{kn}(1-f_{kn'})\sigma(E_{kn'}-E_{kn}-\hbar\omega) \quad (1)$$

where e is the electron charge and m is the mass, ω is the frequency of the incoming electromagnetic radiation, V is the volume of the unit cell, and $(p_x, p_y, p_z)=p$ is the momentum operator $|kn\sigma\rangle$ the crystal wave function, corresponding to eigenvalue E_{kn} with crystal momentum k and spin σ. Finally, f_{kn} is the Fermi distribution function ensuring that only transitions from occupied to unoccupied states are counted, and $\sigma(E_{kn'}-E_{kn}-\omega)$ is the condition for total energy conservation. The real part $\varepsilon_1(\omega)$ can be obtained from the imaginary part $\varepsilon_2(\omega)$ using the Kramer's Kronig dispersion relation [36].

$$\varepsilon_1(\omega)=1+\frac{2}{\pi}P\int_0^{\infty}\frac{\omega'\varepsilon_2(\omega')}{\omega'^2-\omega^2}d\omega' \quad (2)$$

In addition we have employed the BoltzTraP code for the calculating the thermoelectric properties, which is based on the analytical expressions of the electronic bands. In the calculation the rigid band approximation and constant relaxation time approximation were also used. We calculated Seebeck coefficients, electrical conductivity, power factor (PF) and resistivity verses the variable temperature.

3. Results and discussion

3.1. Electronic structure

The electronic band structure of Na_3VF_6 is presented in Fig. 2, which show that the nature of the calculated compound is metallic as the valence and the conduction bands are found to cross at the Fermi energy. To the best of our knowledge no comprehensive work neither experimental data or first principles calculations on band structure of this compound have appeared in the literature to make a meaningful comparison.

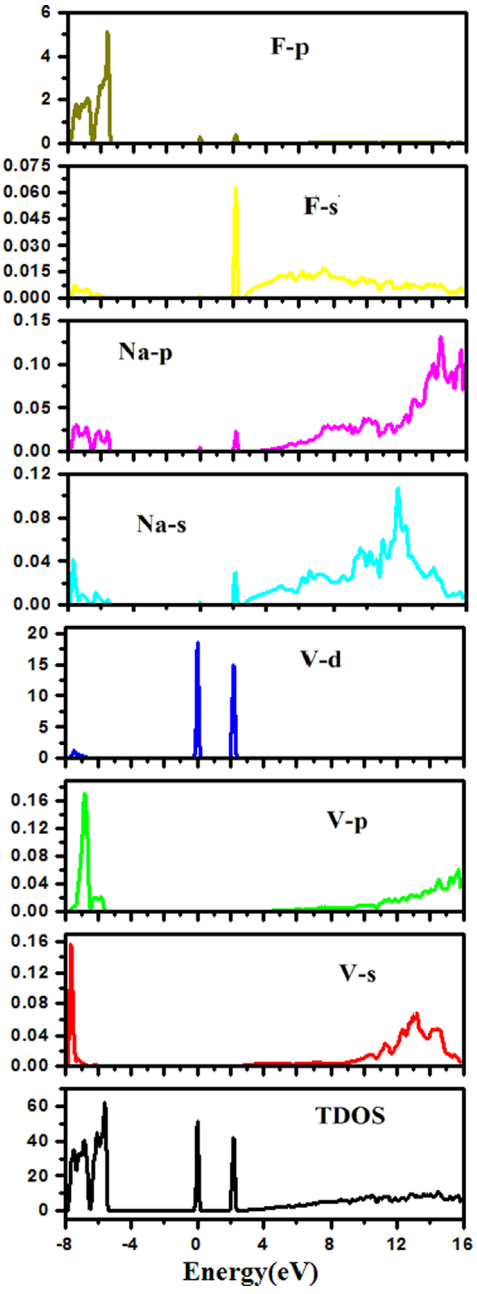

Fig. 3. Calculated total and partial density of state for Na_3VF_6 compound (State/eV unit cell)

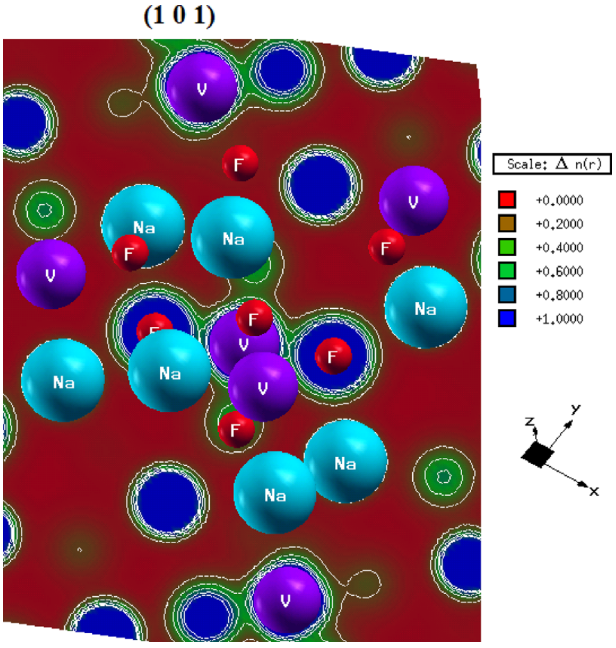

Fig. 4. Calculated electron charge density for Na_3VF_6 compound.

It is important to understand the nature of electronic states around the Fermi surface. The DOS at the Fermi energy (E_F) is assessed by the overlapping of V-d state, with a DOS at $E_F - N(E_F)$ of about 18.655, 51.932 and 13.235 states/eV for LDA, GGA and EVGGA, respectively. We inflate the band structure near E_F to highlight the overlapping of the bands around E_F (see Fig. 2). The obtained data also allowed us to estimate the Summerfield constants (γ) for Na_3VF_6 compound under the assumption of the free electron model as

$$\gamma = \frac{1}{3}\pi^2 N(E_F) K_\beta^2$$

where $N(E_F)$ is the DOS at E_F and K_β is the Boltzmann constant. The deliberated density of states at the Fermi energy permits us to calculate the bare electronic specific heat coefficient, which is 3.236 mJ/mol-K^2, 9.008 mJ/mol-K^2 and 2.295 mJ/mol-K^2 for LDA, GGA AND EVGGA, respectively.

The calculated total density of states (TDOS) and partial density of states (PDOS) for Na_3VF_6 are plotted in Fig. 3. The density of states shows that V-s/p and F-p states are more significant than the Na-s/p states at lower energies i.e. between −8.0 eV and −4.0 eV. The Fermi level is assessed by the overlapping of V-d state. At lower conduction band energies i.e. from 1.0 eV to 3.0 eV the V-d and F-s states are more significant than the Na-s/p state. There is a strong hybridization between Na-s and Na-p states at lower energies of the conduction band. To visualize the chemical bonding nature between the constituents of Na_3VF_6, we have calculated the distribution of charge density in the (1 0 1) plane. We have plotted the charge density contour in the (1 0 1) plane as illustrated in Fig. 4. The figure shows a sharing of charge between V and F, thus there is covalent bonding between V and F atoms. The spherical charge distribution around the sodium site indicates the ionic bonding of Na.

3.2. Fermi surface

The detention of the electronic states at the Fermi level formulates it clear that the nature of the material is metallic. So it is important to set up the shape of the Fermi surface (FS). We have studied the FS of Na_3VF_6 by using the FPLAPW method as shown in Fig. 5, which illustrates the bands around Fermi level. It is seen that the Fermi level is crossed by V-d state, which specifies that the electrical conductivity of this phase should be metallic. The electrons closest to the Fermi level are responsible for conductivity; the electronic structure of any metallic material is understandable from the Fermi surface (FS). We have shown the Fermi surface of Na_3VF_6, in order to get a better report of the states crossing the Fermi level. The shaded region in the FS shows the electronic sheets and the empty space shows the holes [37–42]. So the FS of Na_3VF_6 contains both holes and electronic sheets because this compound contains both empty and shaded region [38,39]. There are two bands crossing the E_F level. The relevant Fermi surface (FS) structures ensuing from these two bands are depicted in Fig. 5. The Fermi bands display an intricate “mixed” character: concurrently with quasi-flat bands along B–C points of the Brillouin zone, a series of high dispersive bands intersects the Fermi level. Fermi surface defines various electrons in the system, whose topology is instantly related to the transport features of materials, such as electrical conductivity.

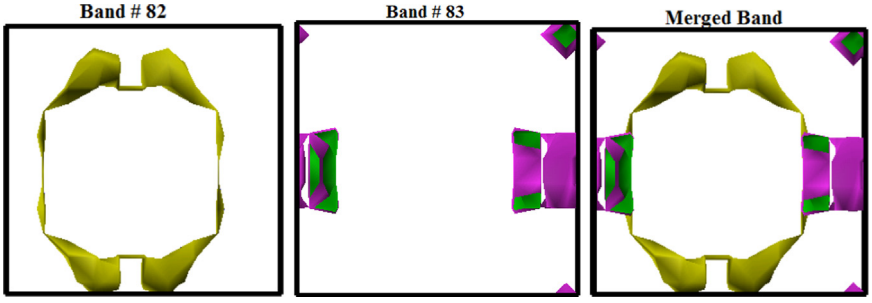

Fig. 5. Calculated Fermi surface for Na_3VF_6 compound.

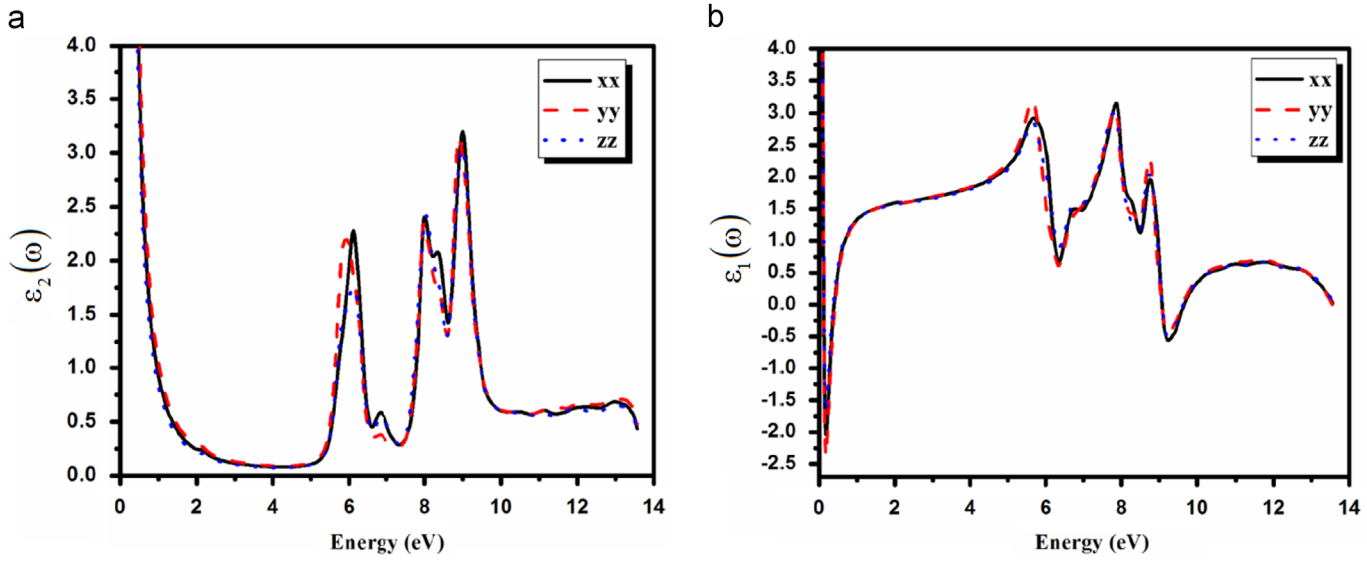

Fig. 6. Calculated imaginary part ($\varepsilon_2(\omega)$) and real part ($\varepsilon_1(\omega)$) of dielectric function for Na_3VF_6 compound.

3.3. Optical properties

In Fig. 6, we have displayed the calculated imaginary and real parts of the dielectric function for Na_3VF_6 as a function of the photon energy from 0.0 eV to 14.0 eV. The dielectric function $\varepsilon = \varepsilon_1 + \varepsilon_2$ spectra will help in accounting for the optical transitions in Na_3VF_6 compound. The imaginary part of the dielectric function, ε_2, was calculated from the direct interband transitions. Fig. 6 shows that there is a prominent structure in the imaginary part of the dielectric function depicted by peaks from 5.5 eV to 10.0 eV and then the decrease occur in the peaks with increase in energy. The structures at about 1.0 eV is associated with direct interband transitions. From band structure results, the transitions originate from the occupied V-d bands to the F-s state. It is seen that the real part of the dielectric function of the compound has a maximum at less than 1.0 eV and then decreases goes to negative which shows that the region below 0.0 eV shows the reflectivity i.e. this region shows the metallic behavior of the material and the region above 0.0 eV shows the transmission of the light. The real part has the prominent peaks at 5.0 eV to 8.0 eV and then decreases sharply and passing through zero at about 9.0 eV. This is probably due to strong interband transitions from deeper lying valence bands to unoccupied bands above the Fermi level.

Fig. 7a and b, shows the real and imaginary parts of the optical conductivity $\sigma(\omega) = \sigma_1(\omega) + i\sigma(\omega)$. In the spectral region at to 10.0 eV there exist a maxima in the conductivity spectra which can be assigned to optical transitions from occupied V-d states to unoccupied F-s state. The reflectivity spectrum is displayed in Fig. 7c. It is noticed that the reflectivity is less than 30% in this compound within the energy range studied. This implies that the material is not a good reflector. At low energies i.e. 2.0 eV to 5.0 eV the spectra shows zero reflectance and then there is however a steady increase in the reflectivity of the compound with increase in energy and after specific increase in the spectra there is again decrease in the spectra at high energies.

3.4. Thermoelectric properties

From the Singh research [43], the enormity of thermo-power can be reduced at elevated temperatures and a squat doping owing to the recompense flanked by holes and electrons when the band gap is diminutive, for example, in PbTe [43]. The principal role begin to play the electron–phonon anharmonicity [44–46] following the photoinduced nonlinear optical analysis.

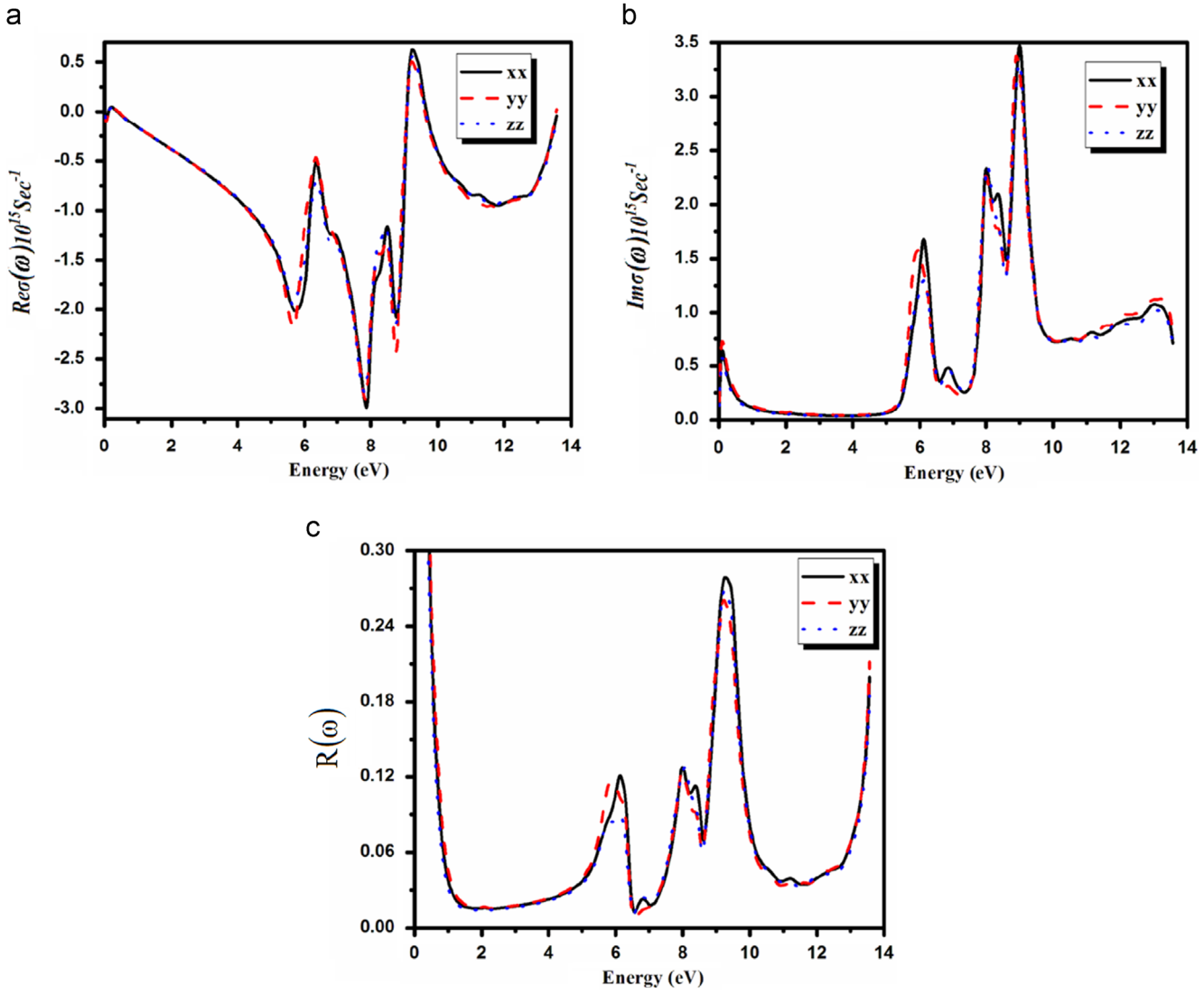

Fig. 7. Calculated optical conductivity and reflectivity.

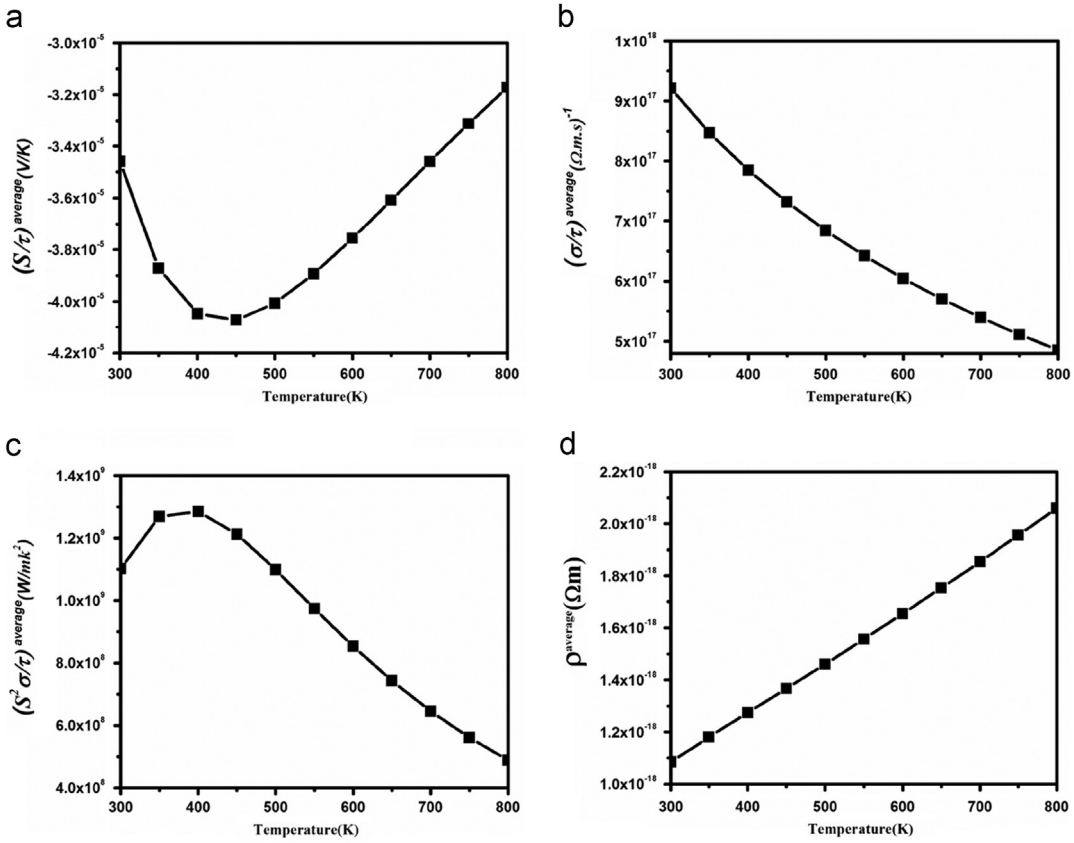

Fig. 8. Calculated thermal properties.

We have calculated the electronic transport coefficients by ensuing the rigid band approximation (RBA) [47,48]. According to the RBA, by doping the band structure does not change but the chemical potential is only changed. This approximation is widely used in theoretical calculations of transport properties of doped semiconductors and is a reasonably good approximation when the doping level is not very large [47–49,50,51]. In addition to the RBA they also assume the relaxation time τ to be energy independent. In this limit, the Seebeck coefficient is independent of τ and therefore any T dependence of τ should not contribute to the T dependence of S. Thus the T dependence of S discussed in this article should be reasonably realistic. However, for a proper understanding of the T dependence of the electrical conductivity and the electronic contribution to the thermal conductivity, one needs to understand the different mechanisms (electron phonon and electron-impurity scattering) contributing to τ, their relative strengths and their T dependence [49,42,52]. Since we do not have a detailed theory of $\tau$for the under investigated compound at the present time we will calculate Seebeck coefficient, electronic conductivity and power factor in units of τ to see how they depend on temperature.

In Fig. 8, we have plotted the Seebeck coefficient, electrical conductivity, power factor and resistivity verses the variable temperatures. The temperature dependent Seebeck coefficient of Na_3VF_6 is shown in Fig. 8a. At room temperature it has a large n-type Seebeck coefficient. And then the magnitude of the Seebeck ($|S|$) rapidly decreasing toward its minimal from 300 K. Electrons being the majority carrier are consistent with their higher mobility. A gradual decrement of the thermopower is due to the thermal excitation of electrons across the Fermi level.

The investigated compound has negative S, the calculated spectra for the Seebeck coefficient shows a different feature at room temperature i.e. at 300 K the value of S is -3.5×10^{-5} but as the temperature increases the graph moves towards the decreasing side and it reaches to its minimum values -4.1×10^{-5} at 450 K temperature. But again increases with a nearly linear increase in magnitude with temperature, aspects which are consistent with degenerate electron transport.

Within the framework of the Boltzmann transport equation in constant relaxation time (τ) approximation, the electrical conductivity (σ) is expressed in the form of the ratio σ/τ. To calculate the electrical conductivity σ, we must determine the relaxation time τ. We assume that the relaxation time τ is direction independent, and treat relaxation time as a constant at a certain specific temperature and carrier concentration. Fig. 8b shows the calculated electrical conductivity. The results follow the trend that the electrical conductivity decreases with increasing temperature and it exhibits metal-like behavior. From the σ/τ values, we obtained a set of the temperature dependent relaxation times as shown in Fig. 8b. The relaxation time shows a decreasing trend with increasing the temperature due to the reduction of mobility at the higher temperature. As we see that by increasing the temperature the conductivity of the investigated material decreases.

The computed power factor (PF) spectra have been shown in Fig. 8c. The spectra shows that at 300 K temperature the power factor value is 1.1×10^{9} but with increasing the temperature the PF increases and reaches to its maximum value at 400 K which is about 1.3×10^{9} and beyond this temperature (400 K) the spectra again shows decrease with increasing the temperature. This confirms that at 400 K this material shows good thermoelectric properties. This material can be use as a good thermo-electric at 400 K temperature.

Fig. 8d shows the temperature dependent electrical resistivity of Na_3VF_6. The spectra show a gradual increase in the resistivity scale with increasing the temperature. It shows metallic-like behavior, at room temperature i.e. at 300 K temperature the resistivity of the material is $1.1\times10^{-18}\ \Omega$ cm.

4. Conclusion

We performed thorough explorations on the electronic structure and Fermi surface Na_3VF_6 compound within a framework of DFT based on full potential calculations. The investigated compound holds metallic character. The Fermi energy (E_F) is evaluated by the overlap of V-d state, with DOS at E_F, $N(E_F)$, of about 18.655, 51.932 and 13.235 states/eV for LDA, GGA and EVGGA, respectively. The bare linear low-temperature electronic specific heat coefficient (γ) is found to be 3.236 mJ/mol-K^2, 9.008 mJ/mol-K^2 and 2.295 mJ/mol-K^2 for LDA, GGA AND EVGGA, respectively. The chemical bonding properties were illuminated by the study of the electronic charge density contour in the (1 1 0) plane. The calculation for the Fermi surface (FS) of Na_3VF_6, suggest that the two bands crossing along the B−C direction. The dielectric functions, imaginary and real parts were calculated. A considerable anisotropy was found between the three components of the imaginary and real parts of the electronic dielectric function. We perceived that in the imaginary and real parts of the electronic dielectric function of Na_3VF_6 compound there subsists a sharp rise below 1.0 eV. We also calculated the thermal properties; from the Seebeck coefficient and power factor we concluded that this compound is suitable for thermal properties at around 400 K temperature.

Acknowledgement

The result was developed within the CENTEM project, reg. no. CZ.1.05/2.1.00/03.0088, co-funded by the ERDF as part of the Ministry of Education, Youth and Sports OP RDI programme.

References

[1] I.N. Flerov, M.V. Gorev, J. Grannec, A. Tresaud, J. Fluorine Chem. 116 (2002)) 9–14.
[2] M. Ahrens, K. Schuschke, S. Redmer, E. Kemnitz, Solid State Sci 9 (2007) 833–837.
[3] I.N. Flerov, M.V. Gorev, K.S. Aleksandrov, A. Tressaud, J. Grannec, M. Couzi, Mater. Sci. Eng 24 (1998) 81–85.
[4] Q.D. Zhou, B.J. Kennedy, J. Solid State Chem. 177 (2004) 654–659.
[5] E.P. Chicklis, C.S. Naiman, R.C. Folweiler, D.R. Gabbe, J.P. Jenssen, A. Linz, Appl. Phys. Lett. 19 (1971) 119.
[6] V.E. Alter, R. Hoppe, Z. Anorg. Allg. Chem. 421 (1975) 110–120.
[7] W. Massa, Z. Anorg, Allg. Chem. 427 (1976) 235–240.
[8] J.H. Choy, J.Y. Kim, S.J. Kim, J.S. Sohn, Chem. Mater. 13 (2001) 906–912.
[9] A. Caramanian, J.P. Souron, P. Gredin, A. deKozak, J. Solid State Chem. 159 (2001) 234–238.
[10] U. Groß, S. Rü diger, E. Kemnitz, Solid State Sci. 9 (2007) 838–842.
[11] S. Lepouter, D. Boyer, A. Pordevin, M. Doubois, V. Briois, R. Mahiou, J. Solid State Chem. 11 (2007) 3049–3057.
[12] P.Y. Jia, J. Lin, M. Yu, J. Lumin 122–123 (2007) 134–136.
[13] Y.L. Yu, Y.S. Wang, D.Q. Chen, F. Liu, Ceram. Int. 34 (2008) 2143–2145.
[14] Y.C. Yue, Z.G. Hu, C.T. Chen, J. Cryst. Growth 310 (2008) 1264–1267.
[15] Y. Birol, J. Alloys Compd. 443 (2007) 94–98.
[16] X. Wang, J. Zhuang, Q. Peng, Y.D. Li, Inorg. Chem. 45 (2006) 6661–6665.
[17] Z.H. Jia, H.Q. Su, S.H. Feng, C.S. Shi, Chin. Chem. Lett. 12 (2001) 1047–1050.
[18] P. Parhi, J. Kramer, V. Manivannan, J. Mater. Sci. 43 (2008) 5540–5545.
[19] H. Hu, Z.G. Chen, T.Y. Cao, Q. Zhang, M.X. Yu, Nanotechnology 19 (2008) 375702 (9pp).
[20] R.N. Hua, Z.H. Jia, D.M. Xie, C.S. Shi, Chin. Chem. Lett. 13 (2002) 1021–1024.
[21] Y. Kumashiro, S. Ozaki, K. Sato, Y. Kataoka, K. Hirata, T. Yokoyama, S. Nagatani, K. Kajiyama, J. Solid State Chem. 177 (2004) 537–541.
[22] F.T. You, S.H. Huang, D.W. Wang, Y. Huang, J.H. Xu, J. Rare Earths 24 (2006) 396–399.
[23] J.H. Zeng, Z.H. Li, J. Su, L.Y. Wang, R.X. Yan, Y.D. Li, Nanotechnology 17 (2006) 3549–3555.
[24] X. Wang, Y.D. Li, Angew. Chem. Int. Ed. 42 (2003) 3497–3500.
[25] L. He, Hongming Yuan, Keke Huang, Chen Yan, Guanghua Li, Qiaoru He, Yang Yu, Shouhua Feng, J. Solid State Chem. 182 (2009) 2208–2212.
[26] C.Y Zhao, S.H Feng, Z.C Chao, R.R Xu, C.S Shi, J.Z. Ni, Chem. Commun. 1641 (1996).
[27] C.Y Zhao, S.H Feng, Z.C Chao, R.R Xu, C.S Shi, J.Z. Ni, Chem. Commun (1997) 945–946.
[28] P. Blaha, K. Schwarz, J. Luitz, WIEN97, A Full Potential Linearized Augmented Plane Wave Package for Calculating Crystal Properties, Karlheinz Schwarz, Techn. Universit at Wien, Austria, ISBN:3-9501031-0-4 (1999).
[29] J.P. Perdew, A. Zunger, Phys. Rev. B: Condens. Matter 23 (1981) 5048.
[30] J.P. Perdew, K. Burke, M. Ernzerhof, Phys. Rev. Lett 77 (1996) 3865.
[31] E. Engel, S.H. Vosko, Phys. Rev. B: Condens. Matter 50 (1994) 10498.
[32] A.H. Reshak, S. Azam, Appl. Phys. A, http://dx.doi.org/10.1007/s00339-013-8126-0.
[33] S. Azam, A.H. Reshak, Int. J. Electrochem. Sci. 8 (2013) 10359–10375.
[34] S. Azam, A.H. Reshak, Int. J. Electrochem. Sci. 9 (2014) 445–459.
[35] A.H. Reshak, S. Azam, Int. J. Electrochem. Sci. 9 (2014) 460–477.
[36] W.T. Ching, P. Rulis, Phys. Rev. B: Condens. Matter 73 (2006) 045202.
[37] S. Azam, A.H. Reshak, Physica B 431 (2013) 102–108.
[38] A.H Reshak, S Azam, J. Magn. Magn. Mater. 352 (2014) 72–80.
[39] A.H Reshak, S Azam, J. Magn. Magn. Mater. 345 (2013) 294–303.
[40] A.H Reshak, S Azam, J. Magn. Magn. Mater. 342 (2013) 80–86.
[41] A.H Reshak, S Azam, J. Magn. Magn. Mater. 351 (2014) 98–103.
[42] A.H. Reshak, S. Azam, Int. J. Electrochem. Sci. 8 (2013) 10396–10423.
[43] David J. Singh, Phys. Rev. B: Condens. Matter 81 (2010) 195217.
[44] K. Nouneh, R. Viennois, I.V. Kityk, F. Terki, S. Charar, S. Benet, S. Paschen, Phys. Status Solidi B 241 (2004) 3069–3080.
[45] K. Nouneh, I.V. Kityk, R. Viennois, S. Benet, K.J. Plucinski, S. Charar, Z. Golacki, S. Paschen, J. Phys. D: Appl. Phys 38 (2005) 965–973.
[46] K. Nouneh, I.V. Kityk, R. Viennois, S. Benet, S. Charar, S. Paschen, K. Ozga, Phys. Rev. B: Condens. Matter 73 (2006) 035329.
[47] L. Chaput, J. P. P´echeur, Tobola, H. Scherrer, Phys. Rev. B: Condens. Matter 72 (2005) 085126.
[48] L. Jodin, J. Tobola, H. P. P´echeur, Scherrer, S. Kaprzyk, Phys. Rev. B: Condens. Matter 70 (2004) 184207.
[49] D.I. Bilc, S.D. Mahanti, M.G. Kanatzidis, Phys. Rev. B: Condens. Matter 74 (2006) 125202.
[50] J.M. Ziman, Electrons and Phonons: Theory of Transport Phenomena in Solids, Oxford University Press, London, UK, 1960.
[51] B.R. Nag, Electron Transport in Compound Semiconductors, Springer-Verlag, Berlin, 1980.
[52] Bao-Ling Huang, Massoud Kaviany, Phys. Rev. B: Condens. Matter **77** (2008) 125209.